THE JOURNAL OF PHYSICAL CHEMISTRY B
A JOURNAL OF THE AMERICAN CHEMICAL SOCIETY

pubs.acs.org/JPCB

Article

Dielectric Properties of Water in Charged Nanopores

Thomas R. Underwood* and Ian C. Bourg*

Cite This: J. Phys. Chem. B 2022, 126, 2688−2698

Read Online

ACCESS | Metrics & More | Article Recommendations | Supporting Information

ABSTRACT: In this study, we examine the spectral dielectric properties of liquid water in charged nanopores over a wide range of frequencies (0.3 GHz to 30 THz) and pore widths (0.3 to 5 nm). This has been achieved using classical molecular dynamics simulations of hydrated Na-smectite, the prototypical swelling clay mineral. We observe a drastic (20-fold) and anisotropic decrease in the static relative permittivity of the system as the pore width decreases. This large decrement in static permittivity reflects a strong attenuation of the main Debye relaxation mode of liquid water. Remarkably, this strong attenuation entails very little change in the time scale of the collective relaxation. Our results indicate that water confined in charged nanopores is a distinct solvent with a much weaker collective nature than bulk liquid water, in agreement with recent observations of water in uncharged nanopores. Finally, we observe remarkable agreement between the dielectric properties of the simulated clay system against a compiled set of soil samples at various volumetric water contents. This implies that saturation may not be the sole property dictating the dielectric properties of soil samples, rather that the pore-size distribution of fully saturated nanopores may also play a critically important role.

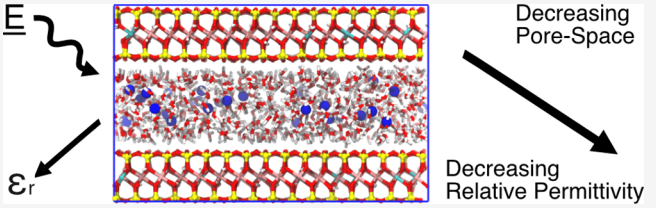

INTRODUCTION

Water is one of the fundamental molecular building blocks of our universe. It plays a predominant role in the evolution of our terrestrial world, the Earth's geology, and the flora and fauna contained within it.[1,2] It has been observed to form large lakes beneath the south pole of Mars[3,4] and is a frequent component of martian soils, trapped within phyllosilicate clay minerals.[5] Recent observations also have discerned water contained within nanoconfined quartz environments on the near side of the moon.[6] It is becoming increasingly apparent that water likely plays an important role in the development of far-off physical environments in addition to those processes typically observed on Earth. Yet, despite its ubiquity and utility within the universe, many mysteries remain regarding its unusual properties.[7,8]

A distinctive property of liquid water is its strong ability to screen Coulomb interactions between charged or polar species.[9] The strong dielectric nature of liquid water is critical to most aspects of life, from Earth's biogeochemical cycles[10,11] to colloidal mechanics[12,13] and solvation, transport, and phase separation in biological structures.[2,14−16] It also underlies the role of water in a vast variety of practical applications, for example, as a sorbent of energy within microwave ovens,[17,18] as a signature for satellite-based radar/remote sensing,[19−23] and as a useful tool in medical diagnostics and therapy,[15] analytical chemistry,[24] geophysical sensing and characterization,[25−27] chemical and pharmacological manufacturing,[24,28,29] and nanofluidic membranes and pumps.[30−32]

A key question, motivated by the importance of interfacial water in natural and engineered systems, is the manner in which the dielectric properties of water are modulated by proximity to nearby surfaces. In essence, how do the static (relative permittivity) and dynamic (dielectric spectral response) properties of water change when near to organic or inorganic interfaces? In the last decade, experimental and computational studies have established that such interfaces can strongly modulate the dielectric properties of liquid water (or even charged species[33]), with important implications in many of the areas outlined above.[25,34,35] The fundamental details of this modulation, however, remain incompletely examined. In particular, most nanoscale examinations of the dielectric properties of water in interfacial or confined environments (with a few exceptions[36,37]) have focused on systems with *pure water* in contact with *uncharged surfaces* including diamond,[38] rutile,[39] silica nanopores,[40] zeolites,[41] graphene nanopores,[42−47] carbon nanotubes,[48,49] and other surfaces.[35,50] In contrast, most water-filled nanopores in biological, geological, and engineered settings have charged pore walls and contain a concomitant, and often high, concentration of counterions.[51,52]

A second important limitation to our present knowledge is that previous examinations of the dielectric properties of confined water have focused almost exclusively on the *static* relative permittivity (also known as the dielectric constant) or on the time scale of the main dielectric relaxation.[25,35,37−40,42−46,50,53] In contrast, the dielectric response of water and aqueous systems takes place over a wide range of

Received: November 9, 2021
Revised: March 11, 2022
Published: April 1, 2022

https://doi.org/10.1021/acs.jpcb.1c09688
J. Phys. Chem. B 2022, 126, 2688−2698

frequencies (up to 15 orders of magnitude[9]) and involves a wide variety of dynamic relaxation and oscillatory modes. The few studies that have examined the dielectric spectra of confined water over a wide range of frequencies have focused relatively narrowly on the dynamics of supercooled water, which are only indirectly topical to most terrestrial environments and engineering solutions,[41,54] or on the main dielectric relaxation mode of liquid water.[49] As will be shown, by ignoring the dynamic dielectric response of water, we miss the detailed mechanistic understanding that underpins the reasons modulating the dielectric response.

In the present study, we aim to provide new insight into the frequency dependent dielectric properties of water in charged nanoconfined environments, including its relative permittivity, static conductivity, and complex dielectric relaxation spectrum. This has been achieved using classical molecular dynamics (MD) simulations of water confined between charged phyllosilicate clay mineral surfaces. These minerals are prototypical natural nanoporous materials that are ubiquitous in terrestrial soils, sediments, and sedimentary rocks, where they contribute roughly half of the solid mass.[55,56] Due to their abundance and fine-grained nature, they strongly influence a wide variety of phenomena including soil fertility, groundwater hydrology, contaminant fate and transport, the global carbon cycle, geomechanics, and plate tectonics.[57−60] Specifically, the simulated systems correspond to the 1-, 2-, and 3-layer hydrate systems that exist within Na-smectite (i.e., the well-known "crystalline" hydrates formed by swelling clay minerals). We also have modeled a larger 5 nm wide nanopore representative of stable "osmotic" hydrate systems. All of these systems are frequently found in nature.[58,61] In addition, we have modeled systems containing bulk liquid water and a 1 M NaCl solution. Overall, our simulations reveal the dielectric response of these systems over 5 orders of magnitude in frequency (from ∼0.3 GHz to 30 THz) and thus provide insight into the dynamics of nanoconfined water in the Earth's subsurface over a wide range of time scales, from femtoseconds to hundreds of picoseconds.

METHODS

Theory. A full description of the theory applied to calculate all quantities in this article can be found within the Supporting Information. Listed below is an abridged description of how each quantity has been calculated from the MD simulations.

The dielectric spectra of each system have been calculated as per Sega et al.[62] as

$$\chi(f) = -\frac{\beta}{3V\epsilon_0}\left[\frac{i}{2\pi f}\int_0^\infty \langle \vec{J}_i(0)\cdot\vec{J}_j(t)\rangle \exp^{-2\pi i f t}\, \mathrm{d}t\right] \quad (1)$$

where $\beta = 1/(k_B T)$ is the inverse thermal energy of the system, V is the system volume, and ϵ_0 is the vacuum permittivity. The quantity $\vec{J}_{\{i,j\}}$ represents the instantaneous current of either the entire system or water, sodium ions, chloride ions, or clay particles, depending upon how one wishes to deconvolute the spectra, defined as

$$\vec{J}(t) = \sum_k^N q_k \vec{v}_k(t) \quad (2)$$

where q_k is the partial charge and $\vec{v}_k(t)$ is the atomic velocity of atom k. The sum counts over all atoms in the species of interest. The key advantage of this method is that one only needs to calculate the current flux of the system, which depends solely on the velocities of the constituent particles, rather than the system's net dipole moment. This is particularly advantageous when free charges are present in the system, since it overcomes the difficulty in calculating the system's dipole moment when free charges jump across periodic boundaries. Once the spectra have been produced, the static relative permittivity has been calculated via fitting the linear regime of the dielectric spectra, at values less than and including 2 GHz.

The static conductivity σ_0, which is a function of the charge flux of ions solely, has been calculated as[37]

$$\sigma_0 = \frac{\beta}{3V\epsilon_0}\int_0^\infty \langle \vec{J}_I(0)\cdot\vec{J}_I(t)\rangle \, \mathrm{d}t \quad (3)$$

where, once again, the conductivity can be deconvolved if one wishes (though this has not been performed in the present study).

Simulation Details. All molecular dynamics simulations have been performed using a custom version of GROMACS 2019.6 modified to output the current of water, cations (Na^+), and anions (Cl^- or clay) at every time step for each system. Brief details of the models used in this study are described below. Full details of the simulation setup, parametrization, and simulation settings can be found in the Supporting Information.

In total, six separate systems were simulated including bulk liquid water, a 1 M NaCl solution, and four nanoconfined environments corresponding to metastable swelling states of a prototypical swelling smectite clay. The clay examined was a Na-montmorillonite with stoichiometry $Na^+_{0.8}[Al_{3.2}Mg_{0.8}]Si_8O_{20}(OH)_4$. The generated nanoconfined environments, referred to as n-layer hydrates (where n represents the number of discrete water monolayers between adjacent mineral surfaces), are presented in the Supporting Information and in our previous work.[63] Specifically, the simulated clay systems correspond to the 1-layer, 2-layer, and 3-layer hydrate systems (the well-known "crystalline" hydrates formed by swelling clay minerals) as well as a larger (5 nm wide) nanopore representative of stable "osmotic" hydrates, all of which are frequently found in nature.[58] The clay minerals have been modeled using the CLAYFF force field,[64] the ions using the Joung−Cheatham parametrization,[65] and the water using the SPC/E parametrization.[66] Recent molecular dynamics simulations of bulk liquid water suggest that the SPC/E water model can accurately reproduce the bulk dielectric properties of water.[67]

For each system, five separate 20 ns replicates were calculated and analyzed to produce data. For the dielectric susceptibility spectra, we used Welch's algorithm to smoothen data by calculating spectra over 1 ns blocks, allowing for 500 ps of overlap between adjacent blocks. A Blackman windowing function was applied in each 1 ns block to minimize spectral leakage. The presented data were then calculated as the average susceptibility spectra of all blocks broken down from each 20 ns simulation (totalling 100 ns worth of data for each simulation setup).

Fitting Procedure. In all cases, calculated spectra have been fitted to physical models using a Levenberg−Marquardt damped least-squares minimization algorithm.[9,14] This process is nontrivial and tends to yield nonunique solutions depending on the fitting approach.[68,69] To minimize the likelihood of overfitting the data, we followed the simplest approach reported in recent studies and modeled our spectra as a sum of two Debye relaxations and two damped harmonic oscillators (DHOs).[14,69]

https://doi.org/10.1021/acs.jpcb.1c09688
J. Phys. Chem. B 2022, 126, 2688−2698

In systems that contain free ions, we additionally included a static conductivity component based on the following equation:

$$\Delta\chi(f) = \chi(f) + \frac{i\sigma_0}{2\pi f} = \epsilon(f) - 1 + \frac{i\sigma_0}{2\pi f} \quad (4)$$

where $\epsilon(f)$ is the complex frequency-dependent relative permittivity ($\epsilon(f) = \chi(f) + 1$) and σ_0 is the static conductivity, defined previously. Full details of our fitting procedure can be found in the Supporting Information, along with the parameters describing the line of best fit for each dielectric spectrum.

RESULTS AND DISCUSSION

Static Relative Permittivity. Static relative permittivities predicted for the six simulated systems are presented in Table 1.

Table 1. Static Relative Permittivities (at 25 °C) Calculated in This Study[a]

system	pore width (nm)	ϵ_r	$\epsilon_{r\parallel}$	$\epsilon_{r\perp}$
water		70.8(1.9)		
1 M NaCl		48.8(9.2)		
5 nm nanopore	5	41.6(5.3)	55.7(7.9)	13.3(0.2)
3-layer hydrate	0.9	22.2(13.9)	30.9(20.8)	4.97(0.02)
2-layer hydrate	0.6	12.1(5.0)	17.7(7.5)	4.07(0.01)
1-layer hydrate	0.3	9.0(2.1)	11.9(3.2)	3.24(0.11)

[a]In confined water systems, results are also presented in directions parallel or normal to the charged mineral surface. For comparison, measured values are ϵ_r = 78.36 for pure water,[70] 66.6 for 1 M NaCl,[74] and ∼5.5 for pure anhydrous smectite clay.[26] The 95% confidence intervals are presented in parentheses.

Our predicted ϵ_r-value for pure water is approximately 10% below the measured value (ϵ_r = 78.36[70]) yet is consistent with previous simulations with the SPC/E water model used in this study (70.7 ± 0.8,[71] 62.6 ± 1.9,[72] 69.9[73]). In 1 M NaCl, our predicted relative permittivity is attenuated by 22% relative to pure water, somewhat more strongly than the 15% attenuation observed in experiments,[74] yet again matching previous simulation results obtained with the SPC/E water model.[73,75]

This dielectric decrement is thought to primarily reflect dielectric saturation in the first hydration shell of ions.[76,77] Its overestimation in our simulations is consistent with the tendency of standard interatomic potential models (such as those used here) to overestimate the impact of ions on water reorientational kinetics.[78]

In nanoconfined environments, ϵ_r decreases with decreasing pore width to well over one-twentieth of the value in bulk liquid water (comparing $\epsilon_{r\perp}$ in the 1-layer hydrate to the bulk liquid water value). Simultaneously, ϵ_r becomes highly anisotropic, with a peak anisotropy in the 3-layer hydrate, where $\epsilon_{r\parallel}/\epsilon_{r\perp}$ = 6.2. Previous experimental data on ϵ_r in this system do not exist, to the best of our knowledge. However, our results are qualitatively consistent with measurements and simulations reported for clay-rich soils (Figure 1a), although these results are generally interpreted as reflecting the saturation state of the soil, whereas our simulations are fully saturated and differ only in pore width. The result suggests that the saturation of a soil may not be the sole dictator of its dielectric properties and that the pore-size distribution of fully saturated nanopores may also play an important role. In addition, our results are broadly consistent with the experimental data set on the dielectric permittivity of water in water-filled slit-shaped boron nitride nanopores (green crosses in Figure 1b), in remarkable agreement with experimental data for water films on mica (pink diamonds in Figure 1b), and with the few existing simulation data sets (red triangles and orange diamonds in Figure 1b). Although it is unsurprising that our results agree with those experimentally measured in mica, it is rather remarkable that we observe qualitative agreement with the other listed studies since the dielectric properties were obtained for very different (uncharged and hydrophobic) materials.

The large confidence intervals presented for our systems in Table 1 are associated with the tendency for the current of free charges (sodium, chloride ions, and clay) to retain a large signal-to-noise ratio over a significant proportion of time within the tail of their autocorrelation (which, as shown in the Supporting Information, influences the calculation of the static relative permittivity). In contrast, the relaxation of the current autocorrelation related to water molecule rotations is not as

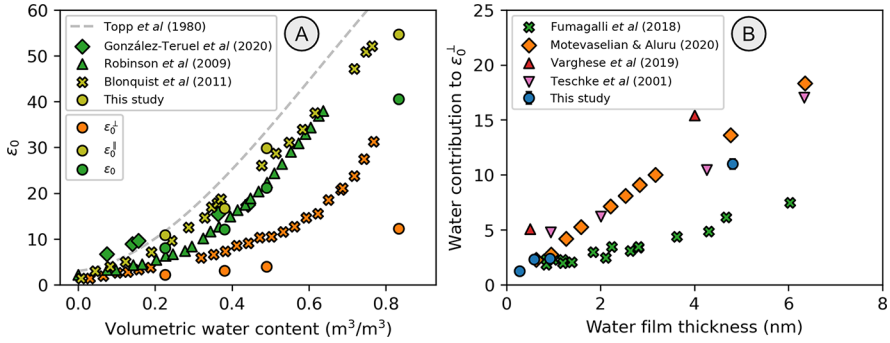

Figure 1. (a) ϵ_r, $\epsilon_{r\parallel}$, and $\epsilon_{r\perp}$ in clay−water mixtures and clayey soils, plotted as a function of volumetric water content. Our results from Table 1 are compared with experimental values obtained for smectite (Gonzalez-Teruel et al.[25]), oriented mica films (Blonquist et al.[79]), and a smectite-rich martian soil analog (Robinson et al.[80]). The relation by Topp et al.[81] describing ϵ_r in nonclayey soils (widely used in dielectric sensing of soil water content) is shown as a dashed line for comparison. (b) Water contribution to $\epsilon_{r\perp}$ in water-filled slit-shaped nanopores, plotted as a function of water film thickness. Our results from Table 2 are compared with the only existing experimental data sets for water in hexagonal boron nitride nanopores (Fumagalli et al.[53]) and on mica (Teschke et al.[12]), and with the only two other existing MD simulation data sets, for water in graphene nanopores (Varghese et al.;[45] Motevaselian and Aluru[47]). We note that the values reported in this study (i.e., the contribution of water to the overall dielectric response of our system) are not exactly equivalent to the other values presented in the figure (which represent the local dielectric constant of water in the thin film) and that the apparent disagreement between previous results in uncharged pores (orange diamonds, red circles, green crosses) is likely due to the use of different definitions of water slab thickness.[82]

https://doi.org/10.1021/acs.jpcb.1c09688
J. Phys. Chem. B 2022, 126, 2688−2698

susceptible to such noise. Moreover, as can be observed in Table 2, the water phase generally contributes the largest proportion to

Table 2. Water Contributions (at 25 °C) to the Static Dielectric Susceptibilities ($\chi_r = \epsilon_r - 1$) Calculated in This Study[a]

system	pore width (nm)	χ_r^{water}	$\chi_{r\parallel}^{water}$	$\chi_{r\perp}^{water}$
water		69.8(1.9)		
1 M NaCl		52.6(1.2)		
5 nm nanopore	5	37.7(1.0)	51.5(1.5)	10.0(0.2)
3-layer hydrate	0.9	15.4(0.7)	22.3(1.1)	1.38(0.10)
2-layer hydrate	0.6	11.4(0.5)	16.4(0.8)	1.31(0.01)
1-layer hydrate	0.3	4.4(0.2)	6.5(0.3)	0.25(0.02)

[a]Note that the 95% confidence intervals (presented in parentheses) are drastically smaller than those presented in Table 1.

the overall dielectric properties of each system. We have highlighted the contributions from water, sodium ions, and clay particles to the overall perpendicular dielectric permittivity $\epsilon_{r\perp}$ in Figure 2. We observe that the large decrement in the dielectric

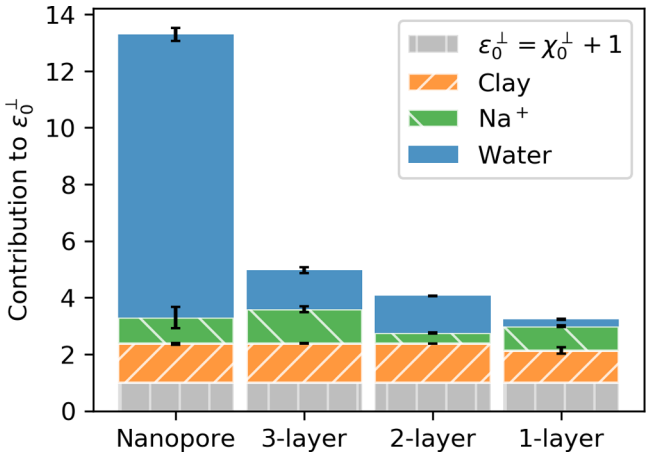

Figure 2. Breakdown of the contributions to the perpendicular static dielectric constant ($\epsilon_{r\perp}$) calculated within the present work. The key contributor to the decrease in static relative permittivity with decreasing pore width is water. The sum of the contributions to χ_r from sodium ions and clay macroions (~2.2 and 3.9 in the directions normal and parallel to the clay surface) is roughly consistent with the measured static dielectric constant of anhydrous smectite clay ($\epsilon_r \approx 5.5$, that is, $\chi_r \approx 4.5$[26]).

screening properties of nanopores is primarily due to the diminishing contribution of the water phase, and as will be shown in a following section, this is due to the suppression of the main Debye relaxation of bulk liquid water. In contrast, we observe that the dielectric contribution to the static permittivity is relatively constant for both sodium ions and larger clay macroions. Finally, we observe the presence of a negative ionic contribution to the relative permittivity of 1 M NaCl solution, noting that the water contribution to the dielectric susceptibility in Table 2 is greater than the overall static dielectric constant presented in Table 1. This result is in keeping with previous molecular simulation results by Sega et al.[83] and with Hubbard and Onsager's proposal of a dynamic decrement to the dielectric properties of dissolved salts in solution.[84]

The long-range impact of confinement on ϵ_r evidenced in Table 1, Table 2, and Figure 1 is remarkable, as most properties of water (including structure, polarization, rotational dynamics, and molecular diffusion) are tangibly impacted by surfaces only over distances <1 nm.[45,85] It is, however, also entirely expected in the context of capacitance models if water has a highly distinct *local* ϵ_r value near surfaces.[53,82] Such models describe the net relative permittivity of a system as a weighted sum of constituent relative permittivities in series akin to a series of capacitors, such that $h/\epsilon^\perp = \sum_i (h_i/\epsilon_i^\perp)$, where h is the system width, i sums over (in this case) two surface-modulated interfacial water films and a separate region of bulk-like liquid water, and $\epsilon_i^\perp$ and h_i are the perpendicular relative permittivity and interfacial width of each phase in the model, respectively. Given a pore or system width of 5 nm, an interfacial film thickness of 0.9 nm, a bulk-like $\epsilon_{bulk}^\perp$ of 70.8, and a system $\epsilon^\perp$ of 11.0 (the water contribution to $\epsilon^\perp$ from Table 2, given $\epsilon_r = \chi_r + 1$) return an interfacial water film relative permittivity of approximately 4.4. In comparison to previous literature, this result is roughly consistent with the value of 2.1 obtained by Fumagalli et al. for 0.9 nm water films on hydrophobic boron nitride substrates.[53] The result further suggests (assuming the applicability of the capacitance model) that the small surface-modulated water film around the mineral surfaces can have relatively long-ranged effects. Applying this model to a 300 nm nanopore, for example, returns a perpendicular dielectric permittivity of 65, only 92% of the value of bulk liquid water.

The distinct dielectric behavior of water near surfaces has, in fact, been previously reported in MD simulation studies that focused on resolving the local static relative permittivity near surfaces.[38−40,43,45] These studies have revealed lower and highly anisotropic values of ϵ_r in the first few monolayers of water near a variety of surfaces including, at least in certain systems, local negative excursions in $\epsilon_{r\perp}$ (i.e., overscreening) in the first water layer[38,39] and $\epsilon_{r\parallel}$ values slightly larger than the bulk water value.[35,43,49] The fundamental explanation of these distinct dielectric properties of interfacial water remains an active area of research[44] and has been variously ascribed to reduced dipole correlations in the perpendicular direction near the surface,[50] in-plane hydrogen-bonding in the first monolayer near uncharged surfaces,[45,47] or dielectric saturation due to high ion concentrations or high electric fields near charged surfaces,[25,36] though its systematic occurrence in a variety of systems suggests that its fundamental origin may be more general.

Overall, our simulation results presented above demonstrate the existence of a large and anisotropic decrease in ϵ_r in clay−water mixtures, one of the most predominant phases in terrestrial soils and sedimentary environments, with potentially important implications, for example, in geophysical sensing.[25,86] This strong dielectric decrement is remarkably similar to that recently reported for two other, very different surfaces: uncharged, hydrophobic hexagonal boron nitride and graphene. In an attempt to further understand the mechanisms driving this dielectric suppression, we now move onto the discussion of the dynamic spectral response of each simulated system. To the best of our knowledge, this has rarely been reported for nanopores containing pure water[49] and not been previously reported for nanopores containing both water and ions.

Dielectric Spectrum of Pure Water. The simulated dielectric susceptibility spectrum ($\chi_r(f) = \chi_r'(f) - i\chi_r''(f)$) of pure water is presented in Figure 3. Overall, the predicted data (gray dots) capture most of the dielectric modes that are observed in the experimental data (yellow curve).[87] We have fitted the calculated spectra as a sum of two Debye relaxations and two damped harmonic oscillators (DHOs) (black curve).

https://doi.org/10.1021/acs.jpcb.1c09688
J. Phys. Chem. B 2022, 126, 2688−2698

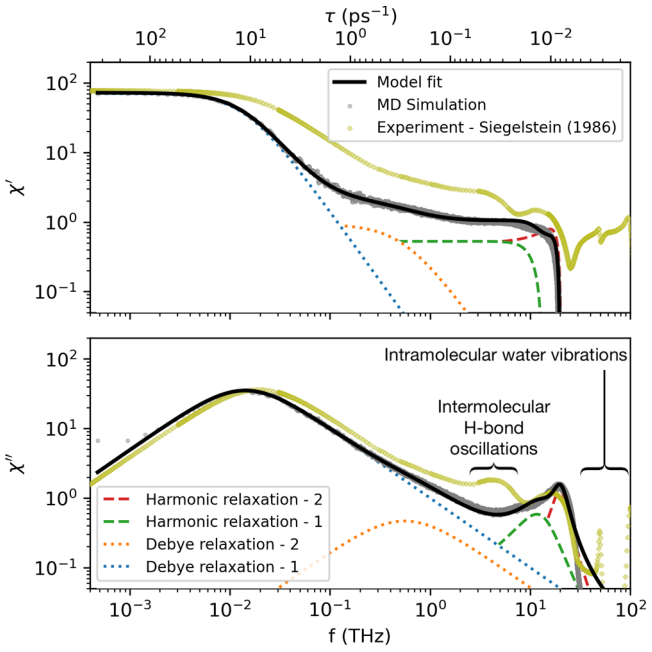

Figure 3. Dielectric susceptibility spectrum of pure liquid water as a function of frequency. Upper and lower panels represent the real and imaginary components. Simulation predictions are presented as gray markers overlaid with a line of best fit presented in black. As noted in the Methods section, the predicted dielectric spectra of water have been broken down into four constitutive terms: two Debye relaxations at lower frequencies and two damped harmonic oscillations (DHOs) at higher frequencies.[14,72,88] The yellow curve is the experimental data set with the most extensive coverage of the frequency range of interest, derived by Elton[69] based on a compilation of refractive index data by Segelstein.[87] Missing contributions to the dielectric spectra of the simulated water correspond to intramolecular water oscillations and to the polarization of water molecules during intermolecular H-bond oscillations.

Full details of our fitting procedure can be read in the Methods section and in the Supporting Information. Notably missing from the predicted spectra are the modes associated with H-bond stretching (at ∼5 THz)[88] and intramolecular vibrations (at >40 THz).[89] Their absence is expressed as missing peaks in the imaginary component (the bottom panel) of the simulated dielectric spectrum at the associated frequencies. These missing peaks in the imaginary part of the spectrum, in turn, cause most of the discrepancy observed in the real component (the top panel) of the calculated spectrum.[69] This effect is entirely expected for simulations carried out with a rigid, nonpolarizable water model[90] (such as the SPC/E model) and can be partially mitigated by running a more costly simulation including flexible intramolecular bonds and polarizable water molecules.[9,90−92]

The largest contribution to the dielectric relaxation of water, contributing approximately 97% of the static relative permittivity of water in our simulations, is a Debye relaxation with frequency f_1 = 14.8 ± 0.4 GHz [$\tau_1 = (2\pi f_1)^{-1}$ = 10.8 ± 0.3 ps] and amplitude S_1 = 67.9 ± 1.9 (see Table S1 in the Supporting Information). The predicted relaxation is ∼30% slower and slightly lower in amplitude than most experimental observations (τ_1 = 8.27 to 8.40 ps,[70,88,93,94] S_1 = 70 to 75[69,93,95]) yet is consistent with previous simulations with the SPC/E water model (τ_1 = 11.0 ± 0.1 ps, S_1 = 68.5 ± 0.7[9]). This mode is generally interpreted as a collective relaxation of the H-bonded water network.[14,69,94,96]

A smaller Debye-like contribution is observed at a higher frequency f_2 = 0.57 ± 0.04 THz (τ_2 = 0.28 ± 0.02 ps) with amplitude S_2 = 0.92 ± 0.05. Early experimental results on this relaxation mode were relatively scattered due to limited frequency coverage,[88,94] but recent results are consistent with our predictions in terms of time scale (τ_2 = 0.25 to 0.42 ps[68,88,95]) while suggesting a greater amplitude (S_2 = 1.45 to 2.8[69,72,93,95,96]), as are previous simulation results with the SPC/E water model (τ_2 = 0.34 ± 0.16 ps, S_2 = 1.5 ± 0.4[9]). This fast relaxation is thought to be associated with H-bond switching events[9,97] and the associated migration of H-bonding defects in the water network.[98]

At higher frequencies, we fit the two dielectrically active librational modes as DHO terms: a less prominent mode at f_3 = 13.15 ± 0.07 THz (wavenumber $\tilde{\nu}$ = 437 cm^{-1}) with S_3 = 0.52 ± 0.00 and a more prominent mode at f_4 = 20.24 ± 0.02 THz (675 cm^{-1}) with S_4 = 0.50 ± 0.01. Our observations are consistent with previous MD simulation results obtained with the SPC/E water model indicating a librational band at ∼20 THz with a "pronounced tail at lower wavenumbers"[9] as well as with previous experimental results (for example, f_3 = 14.7 THz with S_3 = 0.50 based on data spanning only up to 13.6 THz in ref 95 or three modes at 14.0, 18.5, and 22.5 THz with amplitudes of 0.32, 0.19, and 0.08 in ref 69). These modes are generally interpreted as due to the rocking and wagging librational motions of individual molecules.[99,100] More precisely, recent calculations suggest that the peak near 20 THz reflects a contribution of rocking and wagging motions combined with collective effects due to the phonon-like propagation of these modes over distances up to 1.1 nm, while the broad feature near 12 THz reflects interactions between transverse and longitudinal phonons.[91]

Dielectric Spectrum of 1 M NaCl. The imaginary component of the dielectric spectrum of a 1 M NaCl solution is presented in Figure 4 (the real component of all subsequently presented spectra can be seen in the Supporting Information). A key difference between the observed spectra for pure water and 1 M NaCl solution is the presence of the DC-conductivity term at low frequencies (dot-dashed brown line on the left side of Figure 4). The impact of this term and the subsequently calculated static conductivities of each system will be discussed in a later section.

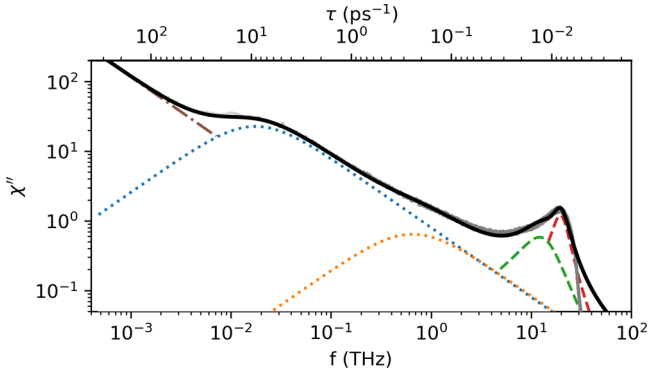

Figure 4. Imaginary component of the dielectric susceptibility spectrum of 1 M NaCl solution as a function of frequency. Simulation predictions are presented and fitted as in Figure 3, with the addition of a DC conductivity term (dot-dashed brown line at low frequencies).

A second key difference is that the main Debye relaxation is attenuated by approximately 35% (in line with the dielectric

https://doi.org/10.1021/acs.jpcb.1c09688
J. Phys. Chem. B 2022, 126, 2688−2698

decrement in ϵ_0 discussed above) and accelerated by 18%. A similar acceleration of the main dielectric relaxation upon addition of 1 M NaCl is reported in experimental studies (by 11%[74] or 15%[76]) and in previous MD simulations with SPC/E water (by 15%[73]). Previous MD simulations have demonstrated that the relaxation time scale τ_1 is highly sensitive to long-range Coulomb interactions[101] as highlighted, for example, by MD simulation results showing a 6-fold decrease in τ_1 when Coulomb interactions were smoothly truncated at ∼0.8 nm[102] and a significant decrease in τ_1 when the main dielectric relaxation was evaluated based on the collective dipole moment evaluated over length scales shorter than ∼1.5 nm.[69] In this context, the observed acceleration of the main dielectric relaxation at high salinity is consistent with the expected tendency of ions to disrupt the long-range Coulomb interactions that stabilize water's hydrogen bond network.

Beyond this, we observe only subtle changes due to NaCl in the higher-frequency portions of the dielectric spectrum. In particular, the amplitude of the fast Debye relaxation is enhanced (as expected if water becomes a less collective medium) while the amplitudes of the two DHO modes decrease by 2% on average (in line with the ∼2% dilution of water when going from pure water to 1 M NaCl). The time scales of these fast relaxations are not impacted by ions, in agreement with studies showing that monovalent ions have little impact on the reorientation kinetics of water molecules beyond their first hydration shell[8,96,103]) and with optical Kerr effect (OKE) measurements indicating that τ_2 has relatively little dependence on salinity in NaCl solutions.[104,105]

Dielectric Spectra in Clay Interlayer Nanopores. Figure 5 presents the imaginary components of the dielectric susceptibility spectra in interlayer clay nanopores. The most notable phenomenon observed here is the dramatic decrease in relative permittivity as a function of decreasing pore spacing, as is also evident with the data presented in Table 1. The key reason for this decrease is the suppression of the major Debye relaxation present in bulk liquid water at ∼20 GHz. This is well evidenced given the decrease in S_1 values (i.e., the amplitude of the primary Debye relaxation mode) with decreasing pore width as presented in the Supporting Information, Table S1, and is further visible in the decreased amplitude of the dotted-blue Debye relaxation in Figure 5.

A second notable phenomenon is the emergence of an additional peak within the 1-layer hydrate (though also discernible in the plots for the 2-layer and 3-layer hydrate) at approximately 700 GHz. This peak does not readily fit either the Debye model or a damped harmonic oscillator. Its origin is associated with the rattling dynamics of interlayer sodium ions as described in the Supporting Information. Because of this new peak, the fitting parameters presented in Figure 5 and Table S1 (Supporting Information) for the fast Debye relaxation should be taken with extreme caution and will not be discussed here. We also note that this peak may be a computational artifact due to potentially inaccurate Na−O surface van der Waals interactions calculated using classical molecular dynamics simulations.[106]

The librational (DHO) modes of water are also somewhat affected by the decreasing pore width. The total intensity of the two librational bands decreases roughly as one would expect based on the decreasing volume fraction occupied by water, with the intensity of the higher-frequency mode decreasing more rapidly than that of the lower-frequency mode with decreasing water content. This observation is also in agreement with Elton and Fernandez-Serra's observation that ice-like phonons exist in

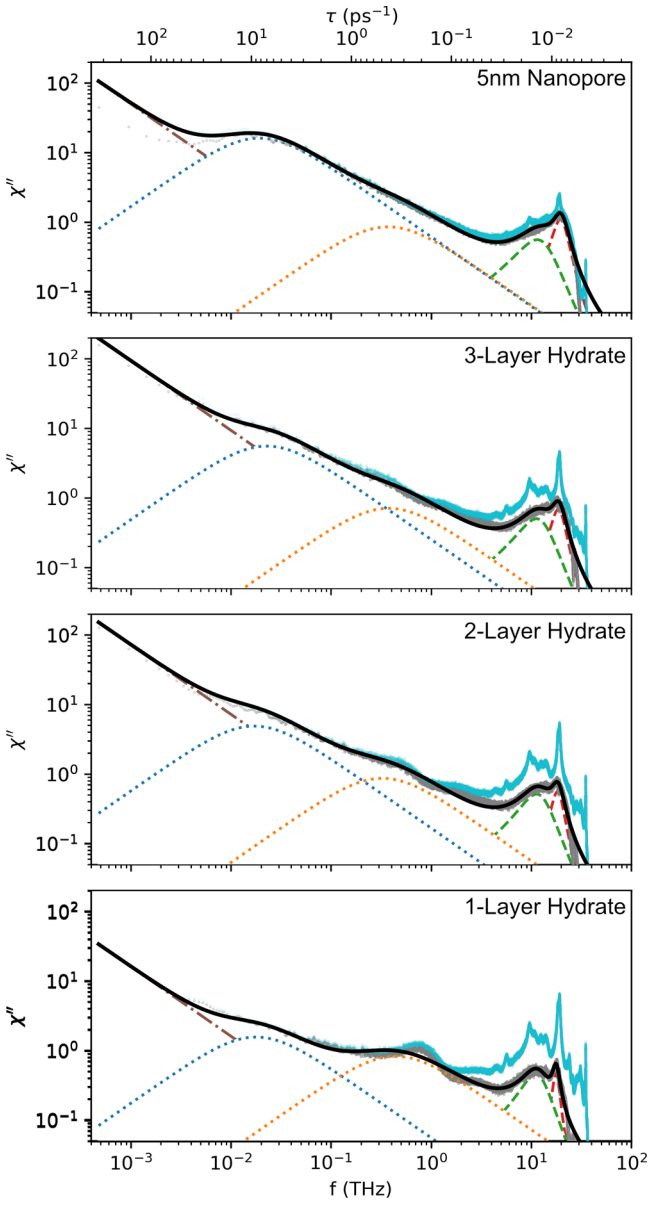

Figure 5. Imaginary component of the dielectric susceptibility spectrum of water and sodium ions in clay interlayer nanopores as a function of frequency (gray dots and fitted black line). The panels show results obtained with different systems in order of decreasing pore width (from top to bottom, 5 nm wide nanopore, 3-layer hydrate, 2-layer hydrate, and 1-layer hydrate). The blue curve shows the total spectrum, including contributions from the clay particles.

liquid water up to distances of 1.1 nm[91] (the pore width of the 3-layer hydrate is only 0.9 nm). Furthermore, the two librational modes shift fairly strongly and consistently toward lower frequencies with decreasing pore width, suggesting a weakening of water hydrogen bonds, in agreement with previous inelastic neutron scattering (INS) and *ab initio* and classical MD simulation studies of the 1- and 2-layer hydrates of Na-smectite.[107,108]

We also observe the presence of major dielectrically active modes due to the presence of the clay mineral. These peaks, presented in blue in Figure 5, have not been fitted but quantitatively agree with previous infrared (IR), inelastic neutron scattering (INS), and *ab initio* and classical MD

https://doi.org/10.1021/acs.jpcb.1c09688
J. Phys. Chem. B 2022, 126, 2688−2698

simulation studies of the vibrational frequency modes present within bulk clay mineral phases.[107−109]

Finally, an important observation is that the relaxation time τ_1 is remarkably insensitive to confinement in our simulated systems. This observation is unexpected based on previous studies where the relaxation time τ_1 was accelerated near low-dielectric surfaces[49] or upon truncation of long-range Coulomb interactions in bulk liquid water.[69,102] The minimal dependence of τ_1 on pore width in our simulations also is remarkable in light of the classical view of water near mineral surfaces as "ice-like",[110−113] which would imply a strong shift of the main Debye relaxation to lower frequencies, with little change in amplitude,[114] and in light of the extensive evidence that the reorientational relaxation of water molecules is slowed significantly (by a factor ∼2 to 7) in contact with a variety of large solutes or interfaces.[2,45,115,116] Our finding on the near-invariance of τ_1 with confinement is supported by the fact that our simulations correctly predict the acceleration of τ_1 with salinity in bulk liquid water.

Further analysis of the dielectric spectra presented in Figure 5, including their deconvolution into contributions from directions parallel and normal to the clay surface or into contributions from water, clay, and sodium self- and cross-interactions is provided in the Supporting Information. We note, in particular, that our deconvolution of the dielectric spectra into contributions from directions parallel and normal to the surface shows a nearly complete disappearance of the main Debye relaxation mode in the direction normal to the surface in all nanoconfined systems. Because of this very strong attenuation, the dielectric relaxation time τ_1 reported here in the direction normal to the surface should be taken with extreme care. In addition, this observation suggests such that the dielectric relaxation time reported in previous studies in directions normal to the surface[43] likely cannot be unambiguously assigned to the collective Debye relaxation of water in the absence of calculations of the full dielectric spectrum.

Static Conductivity. An additional quantity attainable from the calculated dielectric spectra is the static conductivity, related to the linear divergence in the low-frequency regime of the imaginary spectra. Predicted static conductivities of the six simulated systems have been calculated based upon the autocorrelation of charge carriers in the system (see theory and Supporting Information for more details) and are presented in Table 3. Our overall value of 6.91 S m^{-1} in 1 M NaCl solution agrees well with previous experimental results (8.5 S m^{-1})[74] and with simulation results obtained using the SPC/E water model (7.3 S m^{-1}).[75]

Table 3. Static Conductivities (at 25 °C) Calculated in This Study[a]

system	pore width (nm)	σ_0	$\sigma_{0\parallel}$	$\sigma_{0\perp}$
water				
1 M NaCl		6.91(0.40)		
5 nm nanopore	5	2.79(0.48)	3.95(0.71)	0.49(0.05)
3-layer hydrate	0.9	5.20(0.91)	7.73(1.38)	0.14(0.05)
2-layer hydrate	0.6	4.02(0.70)	6.03(1.05)	0.01(0.00)
1-layer hydrate	0.3	0.89(0.14)	1.31(0.21)	0.04(0.00)

[a]In units of Siemens per meter (S m^{-1}). In confined water systems, results are also presented in directions parallel or normal to the clay surface.

We note that a significant contribution to the bulk static conductivity of confined systems arises from the conductivity in the plane parallel to the clay sheets (the *xy*-plane). In contrast, the conductivity perpendicular to the infinite lamellae of clay sheets (the *z*-direction) is rather small, befitting the fact that sodium ions (the primary charge carrier in the clay systems) cannot diffuse freely in this dimension.

We also observe a maximum in the conductivity of nanoconfined systems within the 2- and 3-layer hydrates of Na-smectite. A reason for this can be deduced given the Nernst−Einstein (NE) approximation for static conductivity: $\sigma_0 = (F^2/(RT))\sum_i z_i^2 D_i c_i$, where F is Faraday's constant, R is the molar gas constant, and z_i, D_i, and c_i are the valence, diffusion coefficient, and molar concentration of ion i, respectively. The sodium contribution to each system's static conductivity has been calculated via both the NE approach and the charge-carrier current autocorrelation and is presented in Figure 6 as orange

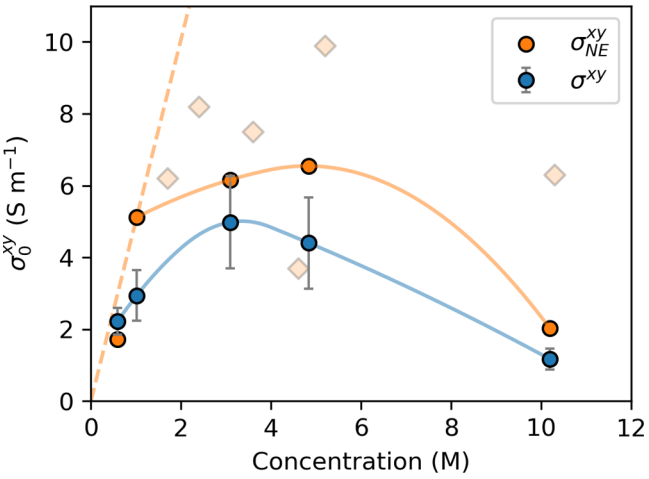

Figure 6. Sodium contribution to the static conductivity of the four simulated clay−water systems and the 1 M NaCl system as a function of sodium concentration (from left to right, 5 nm pore, 1 M solution, 3-, 2-, and 1-layer hydrates). Blue circles show the actual conductivity given via the autocorrelation of charge carriers. Orange circles show values calculated using the NE approximation. Solid orange and blue lines are shown to guide the eye. Orange diamonds show previously reported values calculated for clay interlayer nanopores using the NE approximation.[117]

and blue circular data points, respectively. Also presented with orange diamonds are the data points of Greathouse et al. calculated via the NE equation using diffusion coefficients calculated within confined clay systems via classical MD simulation,[117] as well as the conductivity for sodium using the bulk diffusion coefficient at infinite dilution presented as a dotted orange line. We observe that the static conductivity of each system can be described as a balance of two competing quantities. As the pore width decreases, the overall concentration of sodium concomitantly increases. In contrast, the overall diffusion coefficient of sodium ions decreases rather drastically at small pore separations (notably within the 1-layer hydrate, at concentrations of ∼10 M). This decrease in sodium conductivity at small pore widths (or, equivalently, at high sodium concentrations) is in keeping with the well-known Kohrausch Law relationship between molar conductivity and concentration, as shown in the Supporting Information. It is therefore the balance of ionic concentration with a limited diffusion coefficient that causes the maximum observed in the

https://doi.org/10.1021/acs.jpcb.1c09688
J. Phys. Chem. B 2022, 126, 2688−2698

static conductivity of these nanoconfined systems in the 2-layer and 3-layer crystalline hydrates of sodium-montmorillonite.

Also present in Figure 6 is the systematic overestimation of the static conductivity calculated via the NE equation in comparison to the actual result given by the charge-carrier current autocorrelation. We note that the key difference between the ideal Nernst−Einstein system (i.e., the dotted orange line) and the orange data points is due to the restricted diffusion coefficients apparent upon confinement. The subsequent difference between the NE (orange circles) and actual data points (blue) arise from the couplings between charged species in each system, which further decrease the overall static conductivity of a system and are excluded from the NE calculation.

Finally, we note in passing that in more complex porous materials, the static conductivity presented here gives rise to an additional relaxation mode in the MHz regime of the dielectric spectra due to the so-called Maxwell−Wagner polarization phenomenon. This relaxation, which remains incompletely understood, has the potential to yield useful insight into the microstructure of porous materials including, notably, argillaceous materials such as soils, mudstones, and shales[86,118,119] and will be the focus of a forthcoming study.

CONCLUSIONS

In this study, we have attempted to provide insight into the dielectric properties of liquid water within charged nanoconfined environments. This has been achieved using classical molecular dynamics simulations in combination with recently developed theory for the calculation of dielectric spectra, as well as advanced analysis techniques utilized for the postprocessing of the dielectric spectra. The key observation we note is that the static permittivity of water reduces drastically and in an anisotropic manner under confinement within a charged nanopore. Other notable findings include the observation that confinement has a strong and anisotropic impact on the amplitude of the main dielectric relaxation (S_1) but remarkably little impact on its time scale (τ_1), that water librational bands shift to lower frequency with increasing confinement (suggesting a weakening of hydrogen bonds), that a Na^+ rattling band emerges at narrow pore widths as a detectable signature of ion crowding, and that conductivity trends show a maximum for pore widths of 0.6 to 0.9 nm (the 2- and 3-layer hydrates). Finally, we observe remarkable agreement between the dielectric properties of the simulated clay system against a compiled set of soil samples at various volumetric water contents. This implies that saturation may not be the sole property dictating the dielectric properties of soil samples, rather that the pore-size distribution of fully saturated nanopores may also play a critically important role.

ASSOCIATED CONTENT

Supporting Information

The Supporting Information is available free of charge at https://pubs.acs.org/doi/10.1021/acs.jpcb.1c09688.

Full description of the theory applied to calculate all quantities in this article (PDF)

AUTHOR INFORMATION

Corresponding Authors

Thomas R. Underwood − *Department of Civil and Environmental Engineering, Princeton University, Princeton, New Jersey 08544, United States;* orcid.org/0000-0001-6323-0055; Email: thomas.underwood@princeton.edu

Ian C. Bourg − *Department of Civil and Environmental Engineering and High Meadows Environmental Institute, Princeton University, Princeton, New Jersey 08544, United States;* orcid.org/0000-0002-5265-7229; Email: bourg@princeton.edu

Complete contact information is available at: https://pubs.acs.org/10.1021/acs.jpcb.1c09688

Notes

The authors declare no competing financial interest.

ACKNOWLEDGMENTS

This work was supported by the U.S. Department of Energy, Office of Science, Office of Basic Energy Sciences, Geosciences Program, under Award DE-SC0018419. Molecular dynamics simulations were performed using resources of the National Energy Research Scientific Computing Center (NERSC), which is supported by the U.S. Department of Energy, Office of Science, under award DE-AC02-05CH11231. Additional support was provided by the Princeton School of Engineering and Applied Sciences through the Howard B. Wentz, Jr., junior faculty award. The authors thank M. Sega for guidance on the calculation of the dielectric spectra as well as B. Dazas and B. Gilbert for feedback at early stages of this work. The authors further thank J. A. Greathouse and two anonymous reviewers for their critical evaluation of the manuscript.

REFERENCES

(1) Chaplin, M. Do we underestimate the importance of water in cell biology. *Nat. Rev. Mol. Cell Biol.* **2006**, *7*, 861−866.

(2) Ball, P. Water is an active matrix of life for cell and molecular biology. *Proc. Natl. Acad. Sci. U. S. A.* **2017**, *114*, 13327−13335.

(3) Orosei, R.; Lauro, S. E.; Pettinelli, E.; Cicchetti, A.; Coradini, M.; Cosciotti, B.; Di Paolo, F.; Flamini, E.; Mattei, E.; Pajola, M.; et al. Radar evidence of subglacial liquid water on Mars. *Science* **2018**, *361*, 490−493.

(4) Orosei, R.; Ding, C.; Fa, W.; Giannopoulos, A.; Hérique, A.; Kofman, W.; Lauro, S. E.; Li, C.; Pettinelli, E.; Su, Y.; et al. The global search for liquid water on Mars from orbit: Current and future perspectives. *Life* **2020**, *10*, 120.

(5) Ehlmann, B. L.; Mustard, J. F.; Murchie, S. L.; Bibring, J.-P.; Meunier, A.; Fraeman, A. A.; Langevin, Y. Subsurface water and clay mineral formation during the early history of Mars. *Nature* **2011**, *479*, 53−60.

(6) Honniball, C. I.; Lucey, P. G.; Li, S.; Shenoy, S.; Orlando, T. M.; Hibbitts, C. A.; Hurley, D. M.; Farrell, W. M. Molecular water detected on the sunlit Moon by SOFIA. *Nature Astronomy* **2021**, *5*, 121−127.

(7) Nilsson, A.; Pettersson, L. G. M. The structural origin of anomalous properties of liquid water. *Nat. Commun.* **2016**, *6*, 8998.

(8) Jungwirth, P.; Laage, D. Ion-induced long-range orientational correlations in water: Strong or weak, physiologically relevant or unimportant, and unique to water or not. *J. Phys. Chem. Lett.* **2018**, *9*, 2056−2057.

(9) Sega, M.; Schröder, C. Dielectric and terahertz spectroscopy of polarizable and nonpolarizable water models: A comparative study. *J. Phys. Chem. A* **2015**, *119*, 1539−1547.

(10) Siskin, M.; Katritzky, A. R. Reactivity of organic compounds in hot water: geochemical and technological implications. *Science* **1991**, *254*, 231−237.

(11) Sverjensky, D. A.; Harrison, B.; Azzolini, D. Water in the deep Earth: the dielectric constant and the solubilities of quartz and corundum to 60 kb and 1200 °C. *Geochim. Cosmochim. Acta* **2014**, *129*, 125−145.

(12) Teschke, O.; Ceotto, G.; de Souza, E. F. Interfacial water dielectric-permittivity-profile measurements using atomic force microscopy. *Phys. Rev. E* **2001**, *64*, No. 011605.
(13) Shen, X.; Bourg, I. C. Molecular dynamics simulations of the colloidal interactions between smectite clay nanoparticles in liquid water. *J. Colloid Interface Sci.* **2021**, *584*, 610−621.
(14) Shiraga, K.; Adachi, A.; Nakamura, M.; Tajima, T.; Ajito, K.; Ogawa, Y. Characterization of the hydrogen-bond network of water around sucrose and trehalose: Microwave and terahertz spectroscopic study. *J. Chem. Phys.* **2017**, *146*, 105102.
(15) Ermilova, E.; Bier, F. F.; Hölzel, R. Dielectric measurements of aqueous DNA solutions up to 110 GHz. *Phys. Chem. Chem. Phys.* **2014**, *16*, 11256−11264.
(16) Ball, P. Water as an active constituent in cell biology. *Chem. Rev.* **2008**, *108*, 74−108.
(17) Mingos, D. M. P.; Baghurst, D. R. Applications of microwave dielectric heating effects to synthetic problems in chemistry. *Chem. Soc. Rev.* **1991**, *20*, 1−47.
(18) Kappe, C. O. Controlled microwave heating in modern organic synthesis. *Angew. Chem., Int. Ed.* **2004**, *43*, 6250−6284.
(19) Rosenkranz, P. W. A model for the complex dielectric constant of supercooled liquid water at microwave frequencies. *IEEE Transactions on Geoscience and Remote Sensing* **2015**, *53*, 1387−1393.
(20) Wang, J. R.; Schmugge, T. J. An empirical model for the complex dielectric permittivity of soils as a function of water content. *IEEE Transactions on Geoscience and Remote Sensing* **1980**, *GE-18*, 288−295.
(21) Lorek, A.; Wagner, N. Supercooled interfacial water in fine-grained soils probed by dielectric spectroscopy. *Cryosphere* **2013**, *7*, 1839−1855.
(22) Kneifel, S.; Redl, S.; Orlandi, E.; Löhnert, U.; Cadeddu, M. P.; Turner, D. D.; Chen, M.-T. Absorption properties of supercooled liquid water between 31 and 225 GHz: Evaluation of absorption models using ground-based observations. *Journal of Applied Meteorology and Climatology* **2014**, *53*, 1028−1045.
(23) Park, C. H.; Montzka, C.; Jagdhuber, T.; Jonard, F.; De Lannoy, G.; Hong, J.; Jackson, T. J.; Wulfmeyer, V. A dielectric mixing model accounting for soil organic matter. *Vadose Zone Journal* **2019**, *18*, 190036.
(24) Little, C. A. E.; Orloff, N. D.; Hanemann, I. E.; Long, C. J.; Bright, V. M.; Booth, J. C. Modeling electrical double-layer effects for microfluidic impedance spectroscopy from 100 kHz to 110 GHz. *Lab Chip* **2017**, *17*, 2674−2681.
(25) González-Teruel, J. D.; Jones, S. B.; Soto-Valles, F.; Torres-Sánchez, R.; Lebron, I.; Friedman, S. P.; Robinson, D. A. Dielectric spectroscopy and application of mixing models describing dielectric dispersion in clay minerals and clayey soils. *Sensors* **2020**, *20*, 6678.
(26) Robinson, D. A. Measurement of the solid dielectric permittivity of clay minerals and granular samples using a time domain reflectometry immersion method. *Vadose Zone Journal* **2004**, *3*, 705−713.
(27) Binley, A.; Hubbard, S. S.; Huisman, J. A.; Revil, A.; Robinson, D. A.; Singha, K.; Slater, L. D. The emergence of hydrogeophysics for improved understanding of subsurface processes over multiple scales. *Water Resour. Res.* **2015**, *51*, 3837−3866.
(28) Akiya, N.; Savage, P. E. Roles of water for chemical reactions in high-temperature water. *Chem. Rev.* **2002**, *102*, 2725−2750.
(29) Narayan, S.; Muldoon, J.; Finn, M. G.; Fokin, V. V.; Kolb, H. C.; Sharpless, K. B. "On water": unique reactivity of organic compounds in aqueous suspension. *Angew. Chem.* **2005**, *44*, 3275−3279.
(30) Porada, S.; Sales, B. B.; Hamelers, H. V. M.; Biesheuvel, P. M. Water desalination with wires. *J. Phys. Chem. Lett.* **2012**, *3*, 1613−1618.
(31) Rinne, K. F.; Gekle, S.; Bonthuis, D. J.; Netz, R. R. Nanoscale pumping of water by AC electric fields. *Nano Lett.* **2012**, *12*, 1780−1783.
(32) Cohen-Tanugi, D.; Grossman, J. C. Mechanical strength of nanoporous graphene as a desalination membrane. *Nano Lett.* **2014**, *14*, 6171−6178.
(33) Jiménez-Ángeles, F.; Harmon, K. J.; Nguyen, T. D.; Fenter, P.; de la Cruz, M. O. Nonreciprocal interactions induced by water in confinement. *Physical Review Research* **2020**, *2*, No. 043244.
(34) Muñoz-Santiburcio, D.; Marx, D. Chemistry in nanoconfined water. *Chemical Science* **2017**, *8*, 3444−3452.
(35) Schlaich, A.; Knapp, E. W.; Netz, R. R. Water dielectric effects in planar confinement. *Phys. Rev. Lett.* **2016**, *117*, No. 048001.
(36) Faraudo, J.; Bresme, F. Anomalous dielectric behavior of water in ionic Newton black films. *Phys. Rev. Lett.* **2004**, *92*, 236102.
(37) Sala, J.; Guàrdia, E.; Marti, J. Specific ion effects in aqueous electrolyte solutions confined within graphene sheets at the nanometric scale. *Phys. Chem. Chem. Phys.* **2012**, *14*, 10799−10808.
(38) Bonthuis, D. J.; Gekle, S.; Netz, R. R. Dielectric profile of interfacial water and its effect on double-layer capacitance. *Phys. Rev. Lett.* **2011**, *107*, 166102.
(39) Parez, S.; Předota, M.; Machesky, M. Dielectric properties of water at rutile and graphite surfaces: effect of molecular structure. *J. Phys. Chem. C* **2014**, *118*, 4818−4834.
(40) Renou, R.; Ghoufi, A.; Szymczyk, A.; Zhu, H.; Neyt, J.-C.; Malfreyt, P. Nanoconfined electrolyte solutions in porous hydrophilic silica membranes. *J. Phys. Chem. C* **2013**, *117*, 11017−11027.
(41) Mallamace, F.; Corsaro, C.; Baglioni, P.; Fratini, E.; Chen, S.-H. The dynamical crossover phenomenon in bulk water, confined water and protein hydration water. *J. Phys.: Condens. Matter* **2012**, *24*, No. 064103.
(42) Martí, J.; Nagy, G.; Guàrdia, E.; Gordillo, M. C. Molecular dynamics simulation of liquid water confined inside graphite channels: Dielectric and dynamical properties. *J. Phys. Chem. B* **2006**, *110*, 23987−13994.
(43) Zhang, C.; Gygi, F.; Galli, G. Strongly Anisotropic Dielectric Relaxation of Water at the Nanoscale. *J. Phys. Chem. Lett.* **2013**, *4*, 2477−2481.
(44) De Luca, S.; Kannam, S. K.; Todd, B. D.; Frascoli, F.; Hansen, J. S.; Daivis, P. J. Effects of confinement on the dielectric response of water extends up to mesoscale dimensions. *Langmuir* **2016**, *32*, 4765−4773.
(45) Varghese, S.; Kannam, S. K.; Hansen, J. S.; Sathian, S. P. Effect of hydrogen bonds on the dielectric properties of interfacial water. *Langmuir* **2019**, *35*, 8159−8166.
(46) Jalali, H.; Ghorbanfekr, H.; Hamid, I.; Neek-Amal, M.; Rashidi, R.; Peeters, F. M. Out-of-plane permittivity of confined water. *Phys. Rev. E* **2020**, *102*, No. 022803.
(47) Motevaselian, M. H.; Aluru, N. R. Universal reduction in dielectric response of confined fluids. *ACS Nano* **2020**, *14*, 12761−12770.
(48) Mikami, F.; Matsuda, K.; Kataura, H.; Maniwa, Y. Dielectric properties of water inside single-walled carbon nanotubes. *ACS Nano* **2009**, *3*, 1279−1287.
(49) Mondal, S.; Bagchi, B. Water in carbon nanotubes: pronounced anisotropy in dielectric dispersion and its microscopic origin. *J. Phys. Chem. Lett.* **2019**, *10*, 6287−6292.
(50) Sato, T.; Sasaki, T.; Ohnuki, J.; Umezawa, K.; Takano, M. Hydrophobic surface enhances electrostatic interaction in water. *Phys. Rev. Lett.* **2018**, *121*, 206002.
(51) Eisenberg, B. Interacting ions in biophysics: real is not ideal. *Biophys. J.* **2013**, *104*, 1849−1866.
(52) Faucher, S.; Aluru, N.; Bazant, M. Z.; Blankschtein, D.; Brozena, A. H.; Cumings, J.; de Souza, J. P.; Elimelech, M.; Epsztein, R.; Fourkas, J. T.; et al. Critical knowledge gaps in mass transport through single-digit nanopores: a review and perspective. *J. Phys. Chem. C* **2019**, *123*, 21309−21326.
(53) Fumagalli, L.; Esfandiar, A.; Fabregas, R.; Hu, S.; Ares, P.; Janardanan, A.; Yang, Q.; Radha, B.; Taniguchi, T.; Watanabe, K.; et al. Anomalously low dielectric constant of confined water. *Science* **2018**, *360*, 1339−1342.
(54) Bergman, R.; Swenson, J. Dynamics of supercooled water in confined geometry. *Nature* **2000**, *403*, 283−286.
(55) Bourg, I. C. Sealing shales versus brittle shales: A sharp threshold in the material properties and energy technology uses of fine-grained

https://doi.org/10.1021/acs.jpcb.1c09688
J. Phys. Chem. B 2022, 126, 2688−2698

sedimentary rocks. *Environmental Science and Technology Letters* **2015**, *2*, 255−259.
(56) Ito, A.; Wagai, R. Global distribution of clay-size minerals on land surface for biogeochemical and climatological studies. *Scientific Data* **2017**, *4*, 170103.
(57) Sposito, G.; Skipper, N. T.; Sutton, R.; Park, S.-H.; Soper, A. K.; Greathouse, J. A. Surface geochemistry of the clay minerals. *Proc. Natl. Acad. Sci. U. S. A.* **1999**, *96*, 3358−3364.
(58) Bourg, I. C.; Ajo-Franklin, J. B. Clay, water, and salt: Controls on the permeability of fine-grained sedimentary rocks. *Acc. Chem. Res.* **2017**, *50*, 2067−2074.
(59) Brown, K. M.; Poeppe, D.; Josh, M.; Sample, J.; Even, E.; Saffer, D.; Tobin, H.; Hirose, T.; Kulongoski, J. T.; Toczko, S.; et al. The action of water films at Å-scales in the Earth: Implications for the Nankai subduction system. *Earth and Planetary Science Letters* **2017**, *463*, 266−276.
(60) Rasmussen, C.; Heckman, K.; Wieder, W. R.; Keiluweit, M.; Lawrence, C. R.; Berhe, A. A.; Blankinship, J. C.; Crow, S. E.; Druhan, J. L.; Hicks Pries, C. E.; et al. Beyond clay: towards and improved set of variables for predicting soil organic matter content. *Biogeochemistry* **2018**, *137*, 297−306.
(61) Wilson, J.; Cuadros, J.; Cressey, G. An in situ time-resolved XRD-PSD investigation into Na-montmorillonite interlayer and particle rearrangement during dehydration. *Clays and Clay Minerals* **2004**, *52*, 180−191.
(62) Sega, M.; Kantorovich, S. S.; Arnold, A.; Holm, C. In *Recent advances in broadband dielectric spectroscopy*; Kalmykov, Y., Ed.; Springer: Dordrecht, 2003; pp 103−122.
(63) Underwood, T. R.; Bourg, I. C. Large-scale molecular dynamics simulation of the dehydration of a suspension of smectite clay nanoparticles. *J. Phys. Chem. C* **2020**, *124*, 3702−3714.
(64) Cygan, R. T.; Liang, J.-J.; Kalinichev, A. G. Molecular models of hydroxide, oxyhydroxide, and clay phases and the development of a general force field. *J. Phys. Chem. B* **2004**, *108*, 1255−1266.
(65) Joung, I. S.; Cheatham, T. E. Determination of alkali and halide monovalent ion parameters for use in explicitly solvated biomolecular simulations. *J. Phys. Chem. B* **2008**, *112*, 9020−9041.
(66) Berendsen, H. J. C.; Grigera, J. R.; Straatsma, T. P. The missing term in effective pair potentials. *J. Phys. Chem.* **1987**, *91*, 6269−6271.
(67) Zarzycki, P.; Gilbert, B. Temperature-dependence of the dielectric relaxation of water using non-polarizable water models. *Phys. Chem. Chem. Phys.* **2020**, *22*, 1011−1018.
(68) Beneduci, A. Which is the effective time scale of the fast Debye relaxation process in water? *J. Mol. Liq.* **2008**, *138*, 55−60.
(69) Elton, D. C. The origin of the Debye relaxation in liquid water and fitting the high frequency excess response. *Phys. Chem. Chem. Phys.* **2017**, *19*, 18739−18749.
(70) Kaatze, U. Complex permittivity of water as a function of frequency and temperature. *Journal of Chemical & Engineering Data* **1989**, *34*, 371−374.
(71) Reddy, M. R.; Berkowitz, M. The dielectric constant of SPC/E water. *Chem. Phys. Lett.* **1989**, *155*, 173−176.
(72) Rønne, C.; Thrane, L.; Åstrand, P.-O.; Wallqvist, A.; Mikkelsen, K. V.; Keiding, S. R. Investigation of the temperature dependence of dielectric relaxation in liquid water by THz reflection spectroscopy and molecular dynamics simulation. *J. Chem. Phys.* **1997**, *107*, 5319−5331.
(73) Rinne, K. F.; Gekle, S.; Netz, R. R. Dissecting ion-specific dielectric spectra of sodium-halid solutions into solvation water and ionic contributions. *J. Chem. Phys.* **2014**, *141*, 214502.
(74) Buchner, R.; Hefter, G. T.; May, P. M. Dielectric relaxation of aqueous NaCl solutions. *J. Phys. Chem. A* **1999**, *103*, 1−9.
(75) Sala, J.; Guàrdia, E.; Martí, J. Effects of concentration on structure, dielectric, and dynamic properties of aqueous NaCl solutions using a polarizable model. *J. Chem. Phys.* **2010**, *132*, 214505.
(76) Nörtemann, K.; Hilland, J.; Kaatze, U. Dielectric properties of aqueous NaCl solutions at microwave frequencies. *J. Phys. Chem. A* **1997**, *101*, 6864−6869.
(77) Adar, R. M.; Markovich, T.; Levy, A.; Orland, H.; Andelman, D. Dielectric constant of ionic solutions: combined effects of correlations and excluded volume. *J. Chem. Phys.* **2018**, *149*, No. 054504.
(78) Laage, D.; Stirnemann, G. Effect of ions on water dynamics in dilute and concentrated aqueous salt solutions. *J. Phys. Chem. B* **2019**, *123*, 3312−3324.
(79) Blonquist, J. M.; Robinson, D. A.; Humphries, S. D.; Jones, S. B. Improved dielectric and electrical conductivity anisotropy measurements using TDR in unsaturated mica. *Vadose Zone Journal* **2011**, *10*, 1097−1104.
(80) Robinson, D. A.; Jones, S. B.; Blonquist, J. M.; Heinse, R.; Lebron, I.; Doyle, T. E. The dielectric response of the tropical Hawaiian Mars soil simulant JSC Mars-1. *Soil Science Society of America Journal* **2009**, *73*, 1113−1118.
(81) Topp, G. C.; Davis, J. L.; Annan, A. P. Electromagnetic determination of soil water content: measurements in coaxial transmission lines. *Water Resour. Res.* **1980**, *16*, 574−582.
(82) Loche, P.; Ayaz, C.; Wolde-Kidan, A.; Schlaich, A.; Netz, R. R. Universal and nonuniversal aspects of electrostatics in aqueous nanoconfinement. *J. Phys. Chem. B* **2020**, *124*, 4365−4371.
(83) Sega, M.; Kantorovich, S.; Arnold, A. Kinetic dielectric decrement revisited: phenomenology of finite ion concentrations. *Phys. Chem. Chem. Phys.* **2015**, *17*, 130−133.
(84) Hubbard, J.; Onsager, L. Dielectric dispersion and dielectric friction in electrolyte solutions. I. *J. Chem. Phys.* **1977**, *67*, 4850−4857.
(85) Israelachvili, J.; Wennerstrom, H. Role of hydration and water structure in biological and colloidal interactions. *Nature* **1996**, *379*, 219−225.
(86) Revil, A. Effective conductivity and permittivity of unsaturated porous materials in the frequency range 1 mHz-1 GHz. *Water Resour. Res.* **2013**, *49*, 306−327.
(87) Segelstein, D. J. The complex refractive index of water. Ph.D. thesis, University of Missouri—Kansas City, 1981.
(88) Fukasawa, T.; Sato, T.; Watanabe, J.; Hama, Y.; Kunz, W.; Buchner, R. Relation between dielectric and low-frequency Raman spectra of hydrogen-bond liquids. *Phys. Rev. Lett.* **2005**, *95*, 197802.
(89) Bertie, J. E.; Ahmed, M. K.; Eysel, H. H. Infrared intensities of liquids. 5. Optical and dielectric constants, integrated intensities, and dipole moment derivatives of H_2O and D_2O at 22 °C. *J. Phys. Chem.* **1989**, *93*, 2210−2218.
(90) Neumann, M. Dielectric relaxation in water. Computer simulations with the TIP4P potential. *J. Chem. Phys.* **1986**, *85*, 1567−1580.
(91) Elton, D. C.; Fernández-Serra, M. The hydrogen-bond network of water supports propagating optical phonon-like modes. *Nat. Commun.* **2016**, *7*, 10193.
(92) Martí, J.; Guàrdia, E.; Padró, J. A. Dielectric properties and infrared spectra of liquid water: influence of the dynamic cross correlations. *J. Chem. Phys.* **1994**, *101*, 10883−10891.
(93) Kindt, J. T.; Schmuttenmaer, C. A. Far-infrared dielectric properties of polar liquids probed by femtosecond terahertz pulse spectroscopy. *J. Phys. Chem.* **1996**, *100*, 10373−10379.
(94) Buchner, R.; Barthel, J.; Stauber, J. The dielectric relaxation of water between 0°C and 35°C. *Chem. Phys. Lett.* **1999**, *306*, 57−63.
(95) Yada, H.; Nagai, M.; Tanaka, K. Origin of the fast relaxation component of water and heavy water revealed by terahertz time-domain attenuated total reflection spectroscopy. *Chem. Phys. Lett.* **2008**, *464*, 166−170.
(96) van der Post, S. T.; Tielrooij, K.-J.; Hunger, J.; Backus, E. H. G.; Bakker, H. J. Femtosecond study of the effects of ions and hydrophobes on the dynamics of water. *Faraday Discuss* **2013**, *160*, 171−189.
(97) Zasetsky, A. Y. Dielectric relaxation in liquid water: two fractions or two dynamics? *Phys. Rev. Lett.* **2011**, *107*, 117601.
(98) Popov, I.; Ishai, P. B.; Khamzin, A.; Feldman, Y. The mechanism of the dielectric relaxation in water. *Phys. Chem. Chem. Phys.* **2016**, *18*, 13941−13953.
(99) Walrafen, G. E. Raman spectrum of water: transverse and longitudinal acoustic modes below ≈300 cm^{-1} and optic modes above ≈300 cm^{-1}. *J. Phys. Chem.* **1990**, *94*, 2237−2239.

https://doi.org/10.1021/acs.jpcb.1c09688
J. Phys. Chem. B 2022, 126, 2688−2698

(100) Carey, D. M.; Korenowski, G. M. Measurement of the Raman spectrum of liquid water. *J. Chem. Phys.* **1998**, *108*, 2669−2675.
(101) Alper, H. E.; Levy, R. M. Computer simulations of the dielectric properties of water: studies of the simple point charge and transferrable intermolecular potential models. *J. Chem. Phys.* **1989**, *91*, 1242−1251.
(102) Ohmine, I.; Tanaka, H. Fluctuation, relaxations, and hydration in liquid water. Hydrogen-bond rearrangement dynamics. *Chem. Rev.* **1993**, *93*, 2545−2566.
(103) Tielrooij, K. J.; Garcia-Araez, N.; Bonn, M.; Bakker, H. J. Cooperativity in ion hydration. *Science* **2010**, *328*, 1006−1009.
(104) Turton, D. A.; Hunger, J.; Hefter, G.; Buchner, R.; Wynne, K. Glasslike behavior in aqueous electrolyte solutions. *J. Chem. Phys.* **2008**, *128*, 161102.
(105) Turton, D. A.; Hunger, J.; Stoppa, A.; Thoman, A.; Candelaresi, M.; Hefter, G.; Walther, M.; Buchner, R.; Wynne, K. Rattling the cage: Micro- to mesoscopic structure in liquids as simple as argon and as complicated as water. *J. Mol. Liq.* **2011**, *159*, 2−8.
(106) Ho, T. A.; Criscenti, L. J.; Greathouse, J. A. Revealing transition states during the hydration of clay minerals. *J. Phys. Chem. Lett.* **2019**, *10*, 3704−3709.
(107) Cygan, R. T.; Daemen, L. L.; Ilgen, A. G.; Krumhansl, J. L.; Nenoff, T. M. Inelastic neutron scattering and molecular simulation of the dynamics of interlayer water in smectite clay minerals. *J. Phys. Chem. C* **2015**, *119*, 28005−28019.
(108) Jiménez-Ruiz, M.; Ferrage, E.; Blanchard, M.; Fernandez-Castanon, J.; Delville, A.; Johnson, M. R.; Michot, L. J. Combination of inelastic neutron scattering experiments and ab initio quantum calculations for the study of the hydration properties of oriented saponites. *J. Phys. Chem. C* **2017**, *121*, 5029−5040.
(109) Madejová, J.; Komadel, P. Baseline studies of the clay minerals society source clays: infrared methods. *Clays and Clay Minerals* **2001**, *49*, 410−432.
(110) Odelius, M.; Bernasconi, M.; Parrinello, M. Two dimensional ice adsorbed on mica surface. *Phys. Rev. Lett.* **1997**, *78*, 2855−2858.
(111) Miranda, P. B.; Xu, L.; Shen, Y. R.; Salmeron, M. Icelike water monolayer adsorbed on mica at room temperature. *Phys. Rev. Lett.* **1998**, *81*, 5876−5879.
(112) Sulpizi, M.; Gaigeot, M.-P.; Sprik, M. The silica-water interface: How the silanols determine the surface acidity and modulate the water properties. *J. Chem. Theory Comput.* **2012**, *8*, 1037−1047.
(113) Knight, A. W.; Kalugin, N. G.; Coker, E.; Ilgen, A. G. Water properties under nano-scale confinement. *Sci. Rep.* **2019**, *9*, 8246.
(114) Kaatze, U. Bound water: Evidence from and implications for the dielectric properties of aqueous solutions. *J. Mol. Liq.* **2011**, *162*, 105−112.
(115) Luzar, A. Water hydrogen-bond dynamics close to hydrophobic and hydrophilic groups. *Faraday Discuss.* **1996**, *103*, 29−40.
(116) Fogarty, A. C.; Laage, D. Water dynamics in protein hydration shells: The molecular origins of the dynamical perturbation. *J. Phys. Chem. B* **2014**, *118*, 7715−7729.
(117) Greathouse, J. A.; Cygan, R. T.; Fredrich, J. T.; Jerauld, G. R. Molecular dynamics simulation of diffusion and electrical conductivity in montmorillonite interlayers. *J. Phys. Chem. C* **2016**, *120*, 1640−1649.
(118) Rotenberg, B.; Cadéne, A.; Dufrêche, J. F.; Durand-Vidal, S.; Badot, J. C.; Turq, P. An Analytical Model for Probing Ion Dynamics in Clays with Broadband Dielectric Spectroscopy. *J. Phys. Chem. B* **2005**, *109*, 15548−15557.
(119) Josh, M.; Clennell, B.; Chauchefert, M.; Han, T. Dielectric permittivity and anisotropy of intact multi-saturated organic shales. *SPWLA 57th Annual Logging Symposium (Reykjavik 25−29 June 2016)*; Society of Petrophysicists and Well Log Analysts: 2016; pp 1−14.

https://doi.org/10.1021/acs.jpcb.1c09688
J. Phys. Chem. B 2022, 126, 2688−2698